Shape and oligomerization state of the cytoplasmic domain of the phototaxis transducer II from Natronobacterium pharaonis

Ivan L. Budyak, Vitaliy Pipich, Olga S. Mironova, Ramona Schlesinger, Giuseppe Zaccai, and Judith Klein-Seetharaman

PNAS 2006;103;15428-15433; originally published online Oct 10, 2006;
doi:10.1073/pnas.0607201103

Shape and oligomerization state of the cytoplasmic domain of the phototaxis transducer II from *Natronobacterium pharaonis*

Ivan L. Budyak*†, Vitaliy Pipich‡, Olga S. Mironova*, Ramona Schlesinger*, Giuseppe Zaccai§, and Judith Klein-Seetharaman*¶‖

*Institute for Structural Biology and ‡Institute of Solid-State Research, Research Center Juelich, 52425 Juelich, Germany; †Center for Biophysics and Physical Chemistry of Supramolecular Structures, Moscow Institute of Physics and Technology, Moscow 141700, Russia; §Institute for Structural Biology, 38027 Grenoble Cedex 1, France; and ¶Department of Structural Biology, University of Pittsburgh, Pittsburgh, PA 15260

Communicated by H. Gobind Khorana, Massachusetts Institute of Technology, Cambridge, MA, August 18, 2006 (received for review March 23, 2006)

Phototaxis allows archaea to adjust flagellar motion in response to light. In the photophobic response of *Natronobacterium pharaonis*, light-activated sensory rhodopsin II causes conformational changes in the transducer II protein (pHtrII), initiating the two-component signaling system analogous to bacterial chemotaxis. pHtrII's cytoplasmic domain (pHtrII-cyt) is homologous to the cytoplasmic domains of eubacterial chemotaxis receptors. Chemotaxis receptors require dimerization for activity and are *in vivo*-organized in large clusters. In this study we investigated the oligomerization and aggregation states of pHtrII-cyt by using chemical cross-linking, analytical gel-filtration chromatography, and small-angle neutron scattering. We show that pHtrII-cyt is monomeric in dilute buffers, but forms dimers in 4 M KCl, the physiological salt concentration for halophilic archaea. At high ammonium sulfate concentration, the protein forms higher-order aggregates. The monomeric protein has a rod-like shape, 202 Å in length and 14.4 Å in diameter; upon dimerization the length increases to 248 Å and the diameter to 18.2 Å. These results suggest that under high salt concentration the shape and oligomerization state of pHtrII-cyt are comparable to those of chemotaxis receptors.

archaebacteria | dynamics | halophilic | small-angle neutron scattering

The photosensory system of the halophilic archaeon *Natronobacterium pharaonis* consists of sensory rhodopsin II (pSRII) and transducer II (pHtrII) proteins (1, 2). Upon absorption of a photon, the seven-transmembrane helical membrane protein pSRII undergoes conformational changes that are transmitted to pHtrII (3). pHtrII is composed of two transmembrane helices and a long intracellular domain that has a CheA/CheW kinase-binding site (2). In the light-activated, "repellent" state pHtrII enhances the autophosphorylation rate of CheA, which, in turn, phosphorylates CheY. CheY interacts directly with the flagellar motor switch, which changes the direction of the rotation of the flagellum, resulting in movement away from light. The same "two-component" signal transduction system has been characterized in detail in eubacterial chemotaxis (4, 5).

The 3D structure of the complex between pSRII and the transmembrane domain of pHtrII is known for both the dark, inactive and the light, activated states (6, 7). These structures and EPR spectroscopic studies (8) suggest that conformational changes in pSRII induce a 15° rotation of pHtrII helix II and a 0.9-Å displacement at its cytoplasmic end (7). However, it is not known how this conformational signal is transmitted to the cytoplasmic signaling domain but it likely involves conformational changes in the domain for histidine kinases, adenylyl cyclases, methyl binding proteins, and phosphatases (9). The latter domain is often present in bacterial sensor and chemotaxis proteins and eukaryotic histidine kinases (10). It connects the transmembrane and cytoplasmic signaling domains in the full-length receptor and is known to have highly dynamic characteristics such as found in molten globules (11). Globally dynamic behavior also characterizes a fragment corresponding to the cytoplasmic signaling domain of the chemotaxis aspartate receptor (12). In crystalline form, the structure of the analogous cytoplasmic domain fragment of the chemotaxis serine receptor Tsr-cyt reveals a 200-Å-long coiled-coil dimeric configuration (13). The ability of the cytoplasmic domain to dimerize is important, because full-length chemotaxis receptors function as dimers and it is known that the activity of the aspartate receptor cytoplasmic fragment, Tar-cyt, from *Salmonella typhimurium* is increased in the presence of the leucine zipper dimerization domain (14). In the presence of CheA and CheW, these fragments form higher-order oligomers (15, 16). This property may have implications for signaling *in vivo*, which is believed to occur in large arrays of organized receptor clusters.

Here, we have investigated the ability of pHtrII-cyt to form oligomeric structures by using a combination of chemical cross-linking, analytical gel-filtration chromatography (AGFC), and small-angle neutron scattering (SANS). We find that in dilute buffers the protein is monomeric. Dimers form in the presence of 4 M KCl, whereas the addition of ammonium sulfate induces higher-order aggregation. The dimensions of both monomeric and dimeric pHtrII-cyt deduced from SANS data are consistent with an elongated rod shape as it was observed for the Tsr-cyt dimer in the crystalline state. CD spectra indicate that the dimeric and especially the monomeric rods are highly dynamic.

Results and Discussion

Conformational Preferences of pHtrII-cyt Under Different Conditions. The CD spectrum of purified pHtrII-cyt in PBS lacks evidence for a stable secondary structure (Fig. 1, solid line). The addition of 4 M KCl, which corresponds to the native intracellular environment of halophilic archaea (17, 18), resulted in a spectrum indicating substantial α-helical structure (Fig. 1, dotted line). Stronger α-helical conformation was observed in the presence of ammonium sulfate saturations between 30% and 60% (Fig. 1, dashed-dotted line). To test whether these differences in the CD spectra obtained in PBS with and without KCl or ammonium sulfate result in significant changes in shape and size of the pHtrII-cyt molecules, we conducted AGFC, cross-linking, and SANS experiments.

Author contributions: I.L.B. and J.K.-S. designed research; I.L.B., V.P., and O.S.M. performed research; I.L.B., G.Z., V.P., and J.K.-S. analyzed data; and I.L.B., V.P., R.S., G.Z., and J.K.-S. wrote the paper.

The authors declare no conflict of interest.

Freely available online through the PNAS open access option.

Abbreviations: AGFC, analytical gel-filtration chromatography; SANS, small-angle neutron scattering; SLD, scattering length density; dPBS, deuterated PBS.

‖To whom correspondence should be addressed. E-mail: jks33@pitt.edu.

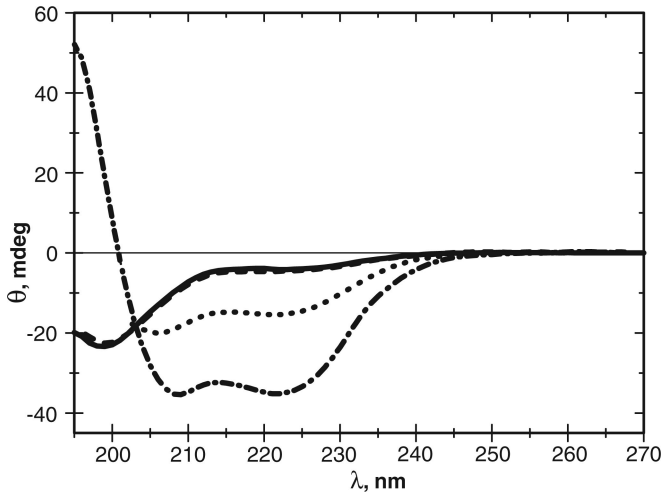

Fig. 1. Far-UV CD spectra of pHtrII-cyt in PBS (solid line), PBS plus 4 M KCl (dotted line), PBS plus 40% ammonium sulfate (dashed-dotted line), and the dimer peak of pHtrII-cyt after cross-linking in PBS plus 4 M KCl in PBS (dashed line).

Analysis of Native pHtrII-cyt by AGFC. AGFC of pHtrII-cyt under different conditions is presented in Fig. 2. All peak fractions were analyzed by SDS/PAGE and confirmed the presence of pHtrII-cyt (data not shown).

In PBS, AGFC shows an elution volume of 11 ml (Fig. 2, m peak). Based on a standard calibration curve obtained with a set of soluble globular proteins, this volume corresponds to a diffusion coefficient of a globular protein with a molecular mass of 240–250 kDa.

Upon the addition of ammonium sulfate to the PBS, a gradual shift of the elution peak to a lower apparent molecular mass was observed (Fig. 2*a*). In 50% and higher saturation of ammonium sulfate, pHtrII-cyt could not be eluted from the column. Subsequent washes with PBS eluted pHtrII-cyt quantitatively (data not shown), which suggests that ammonium sulfate induces aggregation that results in unspecific hydrophobic interactions with the gel-filtration column. In the presence of 4 M KCl or 4 M NaCl, the elution volume of pHtrII-cyt increased from 11.0 to 12.1–12.5 ml and broadened (Fig. 2*b*). The results from AGFC support the conclusion that the solvent-dependent changes in CD spectra (Fig. 1) are associated with changes in shape, size, or aggregation state of pHtrII-cyt.

SDS/PAGE and AGFC of Cross-Linked pHtrII-cyt. Because AGFC alone cannot distinguish between conformational changes and differences in size or aggregation state, we carried out cross-linking experiments in PBS with ammonium sulfate or KCl (Fig. 3). To minimize contributions of conformational changes and differences in solvent interactions to AGFC elution volumes, we conducted all experiments in a single running buffer (PBS). Indeed, the CD spectrum obtained in PBS after cross-linking in different additives returns to that of the monomer in PBS (Fig. 1, dashed line). The SDS/PAGE gels corresponding to the AGFC peaks are shown in Fig. 3 *Insets*. Each peak is labeled with a number that identifies the corresponding band on the SDS gel. The identity of each band was derived from SDS/PAGE of the respective individual fractions from AGFC (data not shown).

On SDS/PAGE, pHtrII-cyt shows a molecular weight higher than the calculated value, indistinguishable from that shown in Fig. 3*a*. This discrepancy is common to the proteins from halophilic archaea (19) and is related to their high negative charge content. To reveal whether there are close homooligomeric contacts between pHtrII-cyt molecules, pHtrII-cyt was incubated with cross-linking reagents, and the SDS/PAGE mobility was analyzed (Fig. 3*a*). Because there was no effect on pHtrII-cyt mobility on SDS/PAGE, we conclude that pHtrII-cyt is predominantly monomeric in PBS. There was no sign of aggregation and/or oligomerization in the range of concentrations used in the experiments. Moreover, AGFC of the cross-linked product in PBS yielded a single major peak eluting at ≈11.3 ml (Fig. 3*a*), similar to the peak at 11.0 ml observed for the uncross-linked sample (Fig. 2, peak m).

The addition of 10% final ammonium sulfate concentration to the cross-linking mixture in PBS did not affect the position of the protein band on SDS/PAGE or the AGFC elution volume (Fig. 2*b*), indicating monomeric configuration. However, both the band on SDS/PAGE and the elution peak became sharper than in PBS. We conclude that ammonium sulfate at low concentrations reduces the polydispersity of pHtrII-cyt without a change in oligomerization state.

In 40% ammonium sulfate, additional bands were seen in SDS/PAGE (Fig. 3*c Inset*). These bands indicated dimer- and higher-order oligomerization. Aggregation was more pronounced in 70% ammonium sulfate (data not shown).

Multiple cross-linked species were observed in 4 M KCl (Fig. 3*d*). When eluting the cross-linked samples during AGFC in PBS, the major intensity was at 10.5 ml (Fig. 3*d*, band 3). This fraction corresponded to a diffuse SDS/PAGE band of molecular mass between 80 and 120 kDa. This molecular mass is approximately double that of the apparent molecular mass of pHtrII-cyt on SDS/PAGE. This result suggests that the majority of pHtrII-cyt is present as a dimer in 4 M KCl or 4 M NaCl (data not shown). When AGFC of the cross-linked sample was repeated in 4 M KCl, higher volumes were required for elution, as observed for the uncross-linked sample (Fig. 2*b*). The major peak in cross-linked pHtrII-cyt was also observed at ≈12.5 ml in

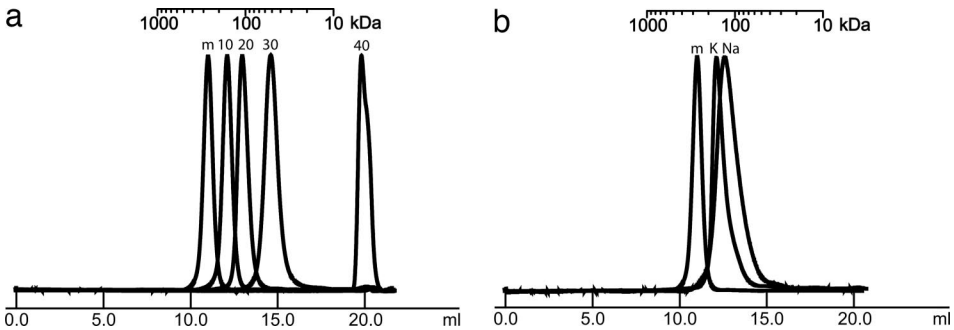

Fig. 2. Effect of salt addition on the elution volumes of pHtrII-cyt on AGFC. m indicates marker peak of pHtrII-cyt in PBS without any additives, 11 ml. (*a*) Effect of ammonium sulfate. The number labels correspond to the ammonium sulfate concentration in % of saturation. (*b*) Effects of 4 M KCl (labeled K) and 4 M NaCl (labeled Na).

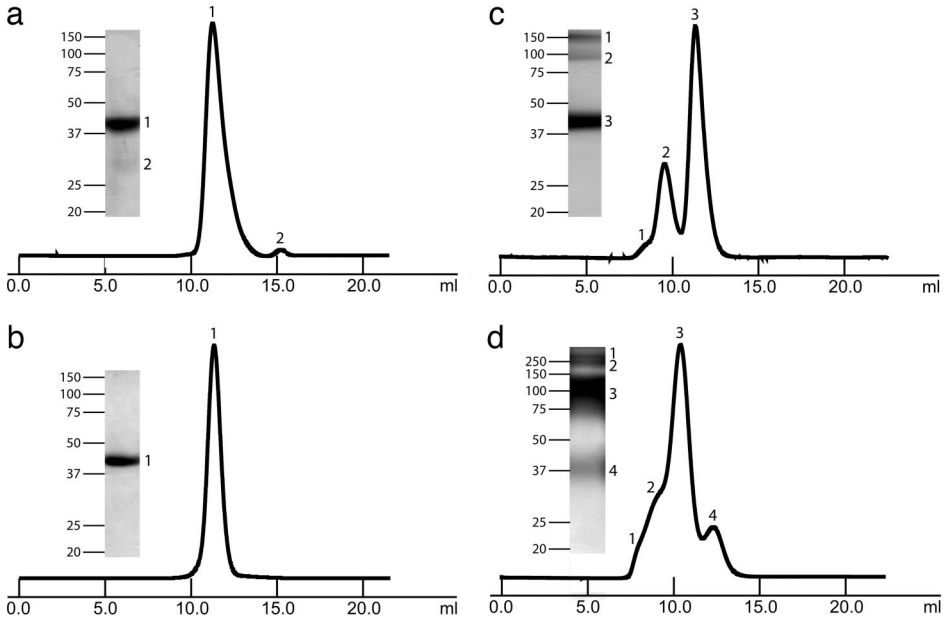

Fig. 3. AGFC and SDS/PAGE (*Insets*) of pHtrII-cyt in PBS after cross-linking with 1-ethyl-3-(3-dimethylaminopropyl)carbodiimide hydrochloride/*N*-hydroxysuccinimide in PBS (*a*), PBS plus 10% ammonium sulfate (*b*), PBS plus 40% ammonium sulfate (*c*), and PBS plus 4 M KCl (*d*).

4 M KCl, whereas it appeared at ≈10.0 ml in PBS alone. This finding indicated that the peak observed at ≈12.5 ml in 4 M KCl in both the cross-linked and uncross-linked samples corresponded to the dimer.

SANS Indicates Rod-Like Shape of pHtrII-cyt. To obtain complementary information on the shape and oligomerization state of pHtrII-cyt, we carried out SANS measurements. In SANS, the scattering intensity $I(Q)$ is proportional to the scattering contrast between the protein particle and the solvent $\Delta\rho^2 = (\rho_p - \rho_{\text{solvent}})^2$, where ρ_p and ρ_{solvent} refer to the scattering length density (SLD) of the particle and the solvent, respectively. For a particle of volume V consisting of atoms with coherent scattering lengths b_i the average SLD ρ is defined as

$$\rho = \sum_i b_i \Big/ V.$$

If we divide the particle into small volume elements v_i and local contrast values ρ_i the radius of gyration R_g is defined as

$$R_g^2 = \sum_i R_i^2 \rho_i v_i \Big/ \sum_i \rho_i v_i,$$

where R_i is the distance from the center of the mass of the contrast distribution in the particle to the volume element i.

Experimental plots of the scattering intensity I as a function of moment transfer value Q are characterized by several regimes: (*i*) the Guinier region ($Q \approx 1/R_g$), which is used to determine R_g; (*ii*) the fractal regime ($Q > 1/R_g$), where the scattering intensity follows a power law $I(Q) \sim Q^{-\alpha}$; and (*iii*) for particles with well defined interfaces the so-called Porod regime (20). The exponent α depends on the shape of the particles. In the Guinier (21) and fractal regimes, scattering curves can be fitted by using the approximation proposed by Beaucage (22):

$$I(Q) = I(0)\exp(-R_g^2Q^2/3) + P[\text{erf}(R_gQ/\sqrt{6})]^3/Q^\alpha, \quad [1]$$

where the first term is the Guinier approximation and P is the amplitude of the power law term. The forward scattering intensity $I(0)$ cannot be measured experimentally directly but is proportional to the scattering contrast:

$$I(0) = \Phi(1 - \Phi)V\Delta\rho^2, \quad [2]$$

where Φ is the volume fraction calculated from the ratio between the protein concentration and the protein density, $\Phi = c/d_p$, and V is the volume of the particle. In the case of rod-like objects ($\alpha = 1$) the amplitude P can be expressed as

$$P = \Phi(1 - \Phi)\pi^2r^2\Delta\rho^2, \quad [3]$$

where r is the radius of the rod.

The scattering intensities of SANS spectra obtained with pHtrII-cyt at concentrations of 2 and 7.5 mg/ml in deuterated PBS (dPBS) were directly proportional to the protein concentration, indicating that the protein does not oligomerize under these conditions. The experimental data normalized by the protein concentration c are plotted in Fig. 4*a* for pHtrII-cyt in dPBS (○) and dPBS plus 4 M KCl (□). In both cases, the scattering intensity $I(Q)$ follows the scaling law Q^{-1} over a wide range of Q values from 0.03 to 0.07–0.1 Å^{-1} (Fig. 4*a*, dashed line). This type of $I(Q)$ dependence is characteristic for dilute randomly oriented rods. Therefore, the experimental observations are consistent with a rod-like shape in both dPBS and dPBS plus 4 M KCl. The radii of gyration R_g were obtained from the linear fits in the Guinier region (Fig. 4*b*). Despite the large differences in secondary structure content, R_g was identical, in both cases being equal to 54 ± 3 Å.

Simulation of Theoretical pHtrII-cyt SANS Data Using the Tsr-cyt Crystal Structure. The Q^{-1} dependence suggests that the shapes of pHtrII-cyt in both dPBS and dPBS plus 4 M KCl correspond to that of a rod. A rod-like shape is consistent with the expectation based on the homologous Tsr-cyt crystal structure shown in Fig. 4*d* (13). We therefore calculated the theoretical scattering curve based on the atomic coordinates from the Tsr-cyt crystal structure (13). The resulting simulated data are plotted in Fig. 4*a* as a dotted line. The shape of the curve approximates the experimental SANS data for pHtrII-cyt in both buffers extremely well. The predicted R_g for Tsr-cyt equals 54.4 Å, which is in excellent

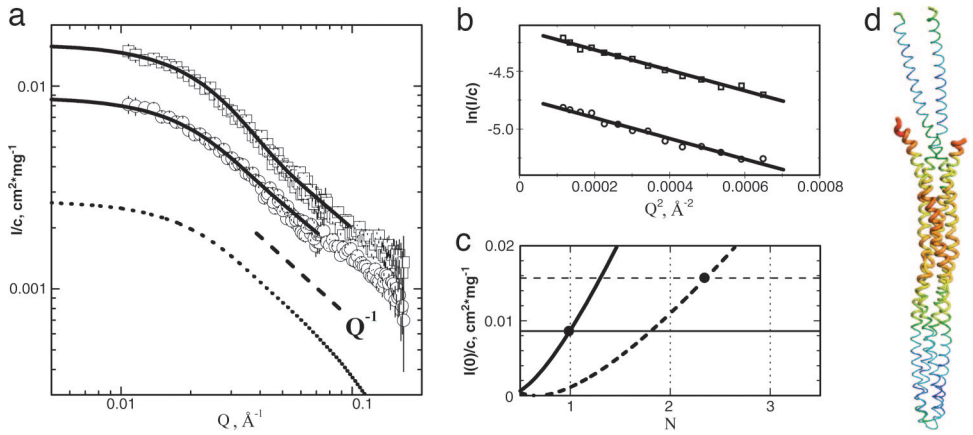

Fig. 4. SANS analysis of pHtrII-cyt in dPBS and dBPS plus 4 M KCl. (*a*) Concentration-normalized SANS data plotted on a double logarithmic scale for pHtrII-cyt in dPBS (○) and dPBS plus 4 M KCl (□). The solid lines correspond to the Beaucage approximation of the experimental data in Eq. **1** (see *Materials and Methods*). The thick dashed line represents the $I(Q) \sim Q^{-1}$ dependence. The dotted line corresponds to the expected SANS curve shape based on the Tsr-cyt crystal structure (see *Materials and Methods*). (*b*) Guinier plots for pHtrII-cyt in dPBS (○) and dPBS plus 4 M KCl (□). The solid lines correspond to the linear fits. (*c*) Dependences of the concentration-normalized forward scattering on the aggregation number. Solid and dashed curved lines represent the modeled dependences for pHtrII-cyt in dPBS and dPBS plus 4 M KCl, respectively. Solid and dashed horizontal lines correspond to the experimentally obtained $I(0)/c$ values. (*d*) X-ray crystal structure model of the cytoplasmic domain fragment of the serine receptor (Tsr-cyt), corresponding to identical positions as the transducer cytoplasmic domain fragment investigated in this study. The Protein Data Bank ID code of Tsr-cyt is 1QU7 (13).

agreement with the experimental values obtained for pHtrII-cyt from the linear fit of the data in the Guinier region.

Oligomerization State of pHtrII-cyt. To determine the aggregation number, N, from the SANS data, we modeled the forward scattering $I(0)$ as a function of N by using Eq. **2**. The overall particle volume V is given by the sum of N monomer volumes V_p plus the solvent shell V_{shell} surrounding the protein. The solvent shell was assumed to be 20% more dense than the solvent and of 3-Å thickness (23), and thus the values for the volume of the solvent shell (V_{shell}) and its SLD (ρ_{shell}) were fixed. The ratio between concentration-normalized forward scattering intensity $I(0)/c$ was plotted as a function of N in Fig. 4*c*. Solid and dashed curved lines in Fig. 4*c* represent pHtrII-cyt in dPBS and dPBS plus 4 M KCl, respectively. Solid and dashed horizontal lines in Fig. 4*c* correspond to the experimentally obtained $I(0)/c$ values, which are also listed in Table 1. Because the error on SANS scattering data in the Guinier region is small (see Fig. 4*b*), the error on extrapolated $I(0)/c$ values is also small (see Table 1). The intersection of experimental and calculated lines gives N. In dPBS, the experimental and theoretical $I(0)/c$ values intersect at $N = 1$. We therefore conclude that pHtrII-cyt in dPBS is in the monomeric form. In dPBS plus 4 M KCl, the intersection is at $N = 2.3$. The fact that N is not an integer value suggests that under these conditions the system is polydisperse. The closest integer number is 2, supporting the conclusion that the majority of particles are dimers with a certain amount of higher-order oligomers and/or aggregates in the solution. Further validation of $N = 2$ comes from comparison of observed scattering intensities and estimated H/D exchange μ in the sample. The number of exchangeable protons from amino acid side chains is 164, and those from the backbone is 271 (24). Based on the assumption that all of these hydrogens are exchangeable (unpublished work), μ is estimated to be <0.223–0.228. For $N = 1$, the experimentally observed $I(0)/c$ value in dPBS corresponds to $\mu = 0.21$. For values $N > 1$, unrealistically high μ values of 0.37 for $N = 2$ and 0.45 for $N = 3$ would be obtained. Thus, the SANS data support the conclusion that in PBS alone pHtrII-cyt is monomeric and mono-disperse, whereas in the presence of 4 M KCl, the equilibrium shifts to a predominantly dimeric state. This conclusion is consistent with that obtained from AGFC and cross-linking.

Dimensions of pHtrII-cyt from SANS Data. Approximating the rod-like structure of pHtrII-cyt to a cylinder, we can estimate the dimensions as follows. Combining $I(0)$ and P from Eqs. **2** and **3**, the length can be calculated directly from the experimental data as $L = \pi I(0)/P$. The length of pHtrII-cyt was estimated to be $L_{PBS} = 202 \pm 5$ Å and $L_{SALT} = 248 \pm 7$ Å in dPBS with and without KCl, respectively. The radius of the cylinder can then be calculated from the aggregation number N, molecular volume of protein chain V_p, and the length of the cylinder L as $r = \sqrt{NV_p/\pi L}$. We obtained cross-sectional diameters $d_{PBS} = 14.4 \pm 0.6$ Å in dPBS and $d_{SALT} = 18.2 \pm 0.8$ Å in dPBS plus 4 M KCl. For comparison, the average cross-sectional diameter of the Tsr-cyt dimer is ≈18 Å. Thus, our data show that in 4 M KCl the overall shape and size of pHtrII-cyt are analogous to those of Tsr-cyt.

Conclusions

Here, we studied the secondary structure, shape, and oligomerization state of the cytoplasmic domain of the phototaxis transducer pHtrII-cyt from the halophilic archaeon *N. pharaonis*. This protein

Table 1. Parameters obtained from SANS experiments

Solvent	c, mg/ml	$I(0)/c$, cm²/mg	P/c, 10^{-4} Å cm²/mg	ρ_p, 10^{10} cm^{-2}	ρ_s, 10^{10} cm^{-2}
dPBS	7.5	0.0086 ± 0.0001	1.33 ± 0.02	3.16	6.34*
dPBS + 4 M KCl	5	0.0157 ± 0.0002	1.98 ± 0.03	2.90	5.10†

c, concentration of the protein in mg/ml; $I(0)/c$, forward scattering normalized by concentration; P/c, scattering amplitude normalized by concentration; ρ_p, SLD of the protein; ρ_s, SLD of the solvent.
*SLD of D_2O ($d = 1.10$ g/cm³).
†SLD of D_2O + 4 M KCl ($d = 1.23$ g/cm³).

domain is analogous to the chemotaxis serine receptor cytoplasmic domain Tsr-cyt for which a crystal structure is available, a dimeric helical coiled-coil that turns back onto itself (13).

A Dynamic Helical Rod Structure for pHtrII-cyt. We expected the structure of pHtrII-cyt to be similar to that of Tsr-cyt, but the CD spectrum in dilute buffer solution (PBS) showed essentially no evidence for helix. Addition of 4 M KCl, considered physiological for *N. pharaonis*, or ammonium sulfate, induces helical structure. On the other hand, SANS data are consistent with the helical coiled-coil rod structure of Tsr-cyt and indicate that the shape in both PBS and 4 M salt is a rod with an R_g of 54 ± 3 Å. This finding suggests that there must be some helix present even in PBS despite the lack of the characteristic 222-nm signal in the CD. This discrepancy poses the question: how much must a helical structure be distorted for the characteristic CD to be lost? Molecular dynamics simulations have shown that both structural dynamics and breaks in the continuity of the helix can cause underestimation of helix content from CD data (25). The "random coil" state as defined by CD spectroscopy is the most elusive conformational ensemble (26, 27). Recent discussions on the prevalence of polyproline II-type configurations in the random-coil ensemble suggest that methods that report on local conformations such as secondary structure estimations using CD and NMR spectroscopy can result in discrepancies to conclusions derived from R_g measurements (28). Taking our SANS estimation of R_g and CD data together, we conclude that pHtrII-cyt is a highly dynamic helical rod. This interpretation in terms of protein dynamics also fits the observed abnormally high elution volume in AGFC. Similar observations were made previously for Tar-cyt from *Escherichia coli*, which elutes at a volume corresponding to 110 kDa (29) and also displays globally dynamic behavior (12). The increased helical content deduced from the CD spectrum of pHtrII-cyt in high salt without changes in R_g estimated from SANS is therefore likely caused by a decrease in conformational flexibility in high salt rather than a folding transition from random coil to helix.

Correlation Between Structural Dynamics and Oligomerization State. Halophilic proteins typically show a correlation between structure and dynamics and oligomerization state and protein function in dependence of salt concentration. For example, malate dehydrogenase from the halophilic archaeon *Haloarcula marismortui* is functional only as a tetramer at high ionic strength. Below 2 M salt, this protein dissociates into monomers and its secondary structure is diminished. This transition is accompanied with a loss of function (30). Consistent with this general observation for halophilic proteins, the changes in structural dynamics we observed for pHtrII-cyt are accompanied by changes in oligomerization state. AGFC, cross-linking, and SANS data indicate that pHtrII-cyt is monomeric in PBS and dimeric in 4 M KCl, whereas ammonium sulfate promotes higher-order aggregation. This finding has likely functional significance, because dimerization is a known requirement for function in chemotaxis receptors and the co-complex of pSRII and the transmembrane domain of pHtrII is a dimer (6). Our studies show that not only the transmembrane helices participate in dimer interactions, but so does the cytoplasmic domain in high salt.

Materials and Methods

Materials. All cloning procedures used *E. coli* strain Top10 (Invitrogen, Carlsbad, CA). Gene expression was carried out in *E. coli* BL21-CodonPlus(DE3)-RIL (Stratagene, La Jolla, CA). *N. pharaonis* strain 2160 cells were obtained from the German Collection of Microorganisms and Cell Cultures (Braunschweig, Germany).

Buffers used were as follows: buffer A, 300 mM NaCl/50 mM NaP_i, pH 8.0; buffer B, 750 mM $(NH_4)_2SO_4$/50 mM NaP_i, pH 6.7; buffer C, 50 mM NaP_i, pH 6.7; PBS in H_2O, 0.9 mM $CaCl_2$/0.5 mM $MgCl_2$/2.7 mM KCl/138 mM NaCl/1.5 mM KH_2PO_4/8 mM Na_2HPO_4; and dPBS, PBS with the same salt composition as PBS, but in D_2O.

All chemicals were obtained from Sigma (St. Louis, MO), unless otherwise stated.

Cloning. The pHtrII sequence was aligned to the Tsr-cyt sequence as in refs. 13 and 31. The starting and end positions of our pHtrII constructs were chosen based on those of Tsr-cyt used in the earlier crystallization experiments (13). Thus, the region of the *htrII* gene corresponding to amino acids 234–504 was amplified by PCR from native *N. pharaonis* cells using 5′-GCGGATCCCATATGGAGGCCAGCGAGGACGTAAAC-3′ as forward and 5′-GCAAGCTTTCAGTCGGCCTGCTCGGAGAGGC-3′ as reverse primers, respectively. The coding DNA fragment was cloned between NdeI and HindIII sites of the vector pET27b+ (Novagen, San Diego, CA). Positive clones were identified by restriction analysis and confirmed by sequencing.

Expression and Purification. For production of pHtrII-cyt protein, transformed *E. coli* BL21-CodonPlus(DE3)-RIL cells were grown in dYT medium containing 50 mg/liter kanamycin at 37°C. When the absorbance at 600 nm reached 0.6–0.8, isopropyl-β-D-thiogalactopyranoside (1 mM) was added to induce expression. After 4 h, the cells were harvested by centrifugation (10,000 × *g*). The cell pellet was resuspended in buffer A, the suspension was passed through a french press (SLM–Aminco, Urbana, IL), and the soluble and insoluble fractions were separated by centrifugation (100,000 × *g*, 1 h, 4°C). The supernatant fraction was subjected to salting out by gradual addition of ammonium sulfate. After each step the sample was incubated for 1 h at 4°C with constant stirring and centrifuged (75,600 × *g*, 30 min, 4°C), and the supernatant solution was used for the next salting-out step. At each step, pellets were resuspended in buffer B. Pellet fractions containing pHtrII-cyt were pooled and applied to a HiTrap Butyl FF column (Amersham Biosciences, Piscataway, NJ). Elution was carried out by using a linear gradient, buffer B to buffer C, and the protein usually eluted at ammonium sulfate concentration between 270 and 150 mM. Gel filtration on HiLoad 26/60 Superdex 200 prep grade column (Amersham Biosciences) served as the last purification step. All fractions were analyzed by SDS/PAGE. Protein concentration was estimated by the bicinchoninic acid protein assay (Pierce, Rockford, IL).

CD Spectroscopy. CD spectra were acquired by using a Jasco 810 spectropolarimeter (Jasco, Easton, MD). Protein solutions containing 0.1 mg/ml pHtrII-cyt in PBS or PBS plus 4 M KCl, or PBS plus 40% ammonium sulfate were placed in a 0.2-cm Hellma (Forest Hills, NY) quartz cell. All spectra were recorded with a bandwidth of 1 nm, scan speed of 100 nm/min, and time constant of 1 s. At least five scans were averaged for each spectrum. The reference spectra, obtained with the samples without protein, were subtracted from the corresponding pHtrII-cyt spectra after acquisition.

AGFC. A Superdex 200 10/300 column (Amersham Biosciences) with separation range for globular proteins between 10 and 600 kDa was used. After preequilibration of the column with the respective buffers, pHtrII-cyt samples (100–500 μl) containing 50 μg were injected and elution was carried out at room temperature at a flow rate of 0.5 ml/min. The absorbance was monitored at 214 nm. Calibration of elution volumes was performed with the soluble globular proteins thyroglobulin (669 kDa), ferritin (440 kDa), BSA (67 kDa), ovalbumin (43 kDa),

and ribonuclease A (13.7 kDa). The reproducibility in elution volumes was ±0.1 ml.

Chemical Cross-Linking. Cross-linking reactions were carried out with solutions of 0.1–0.5 mg/ml pHtrII-cyt in different buffers (see *Results and Discussion*) by addition of 2 mM 1-ethyl-3-(3-dimethylaminopropyl)carbodiimide hydrochloride (Pierce) and 5 mM *N*-hydroxysuccinimide (Pierce) at room temperature (32, 33). The reactions were terminated after 24 h with 10 mM Tris and 20 mM 2-mercaptoethanol, and then the cross-linked products were dialyzed in 3.5-kDa cut-off dialysis bags (Qbiogene, Irvine, CA) against PBS to remove excess of salt and unreacted cross-linkers. The products were analyzed by AGFC and SDS/PAGE.

SANS. The SANS measurements were carried out by using the KWS-I instrument at the FRJ-2 research reactor (Research Center Juelich). A neutron wavelength of $\lambda = 7$ Å with sample-to-detector distances of 2 and 4 m was used to get a range in scattering vector Q values of 0.01–0.2 $Å^{-1}$. Protein samples containing 2 mg/ml and 7.5 mg/ml pHtrII-cyt in dPBS and 5 mg/ml pHtrII-cyt in dPBS plus 4 M KCl were analyzed at room temperature in quartz cells with 1.00-mm path lengths. The data were corrected for the detector efficiency and the scattering from the empty cell and solvent, and then radially averaged and calibrated in absolute units by a Plexiglas secondary standard.

All SANS measurements were carried out in buffers prepared with heavy water to improve signal-to-noise ratios (34). We verified with CD spectroscopy that the exchange of H_2O to D_2O did not cause non-native conformational changes or induce aggregation.

Scattering Curve Modeling. The theoretical SANS curve for the Tsr-cyt crystal structure [Protein Data Bank ID code 1QU7 (13)] was simulated by using the CRYSON (version 2.6) software package (35). Default input parameters were chosen, except for the fraction of exchangeable peptide backbone H atoms, which we assumed to be 100%.

Estimation of Aggregation Number from SANS Data. To estimate the oligomerization state (aggregation number, N), $I(0)$ in Eq. **2** was rewritten assuming scattering volume $V = NV_p + V_{shell}$, scattering volume fraction $\Phi = \Phi_p + \Phi_{shell}$, and scattering contrast $\rho = (\rho_p V_p + \rho_{shell} V_{shell})/(V_p + V_{shell})$ as follows. In a monodisperse system, the aggregation number is given by $N = V_{agg}/V_p$, where V_{agg} is the volume of the aggregate and $V_p = M_p/(N_a d_p)$ is the volume of protein of molar mass M_p, d_p is the density, and N_a is Avogadro's number. Because of the presence of the surrounding hydration shell, $V = NV_p + V_{shell} = NV_p(1 + \lambda)$ with λ being the ratio between the volume of the shell and the volume of the protein aggregate. Similarly, the scattering volume fraction is modulated by the hydration shell also: $\Phi = \Phi_p + \Phi_{shell} = \Phi_p(1 + \lambda)$, where $\Phi_p = c/d_p$. Finally, the SLD of protein plus shell is given by $\rho = (\rho_p NV_p + \rho_{shell} V_{shell})/(NV_p + V_{shell}) = (\rho_p + \rho_{shell}\lambda)/(1 + \lambda)$. In the case of a cylinder the ratio between volume of shell and protein complex λ is a function of the radius r and shell thickness Δ: $\lambda = 2\Delta/r(1 + \Delta/(2r))$ ($r = r_1\sqrt{N}$ and $r_1 = \sqrt{V_p/\pi L}$).

Because we measured the samples in D_2O, we took H/D exchange into account by the "exchange factor" μ in defining SLD as $\rho_p = \mu\rho_p^D + (1 - \mu)\rho_p^H$. The SLD of the fully protonated form ($\mu = 0$), $\rho_p^H = 1.93 \times 10^{10}$ cm^{-2}, was calculated from its chemical formula $C_{1182}H_{1926}O_{487}N_{332}S_7$ and density $d_p = 1.4$ g/cm^3. The fully deuterated form ($\mu = 1$), $\rho_p^D = 7.80 \times 10^{10}$ cm^{-2}, was calculated by using $C_{1182}D_{1926}O_{487}N_{332}S_7$ and $d_p = 1.49$ g/cm^3.

With these modifications, Eq. **2** for the forward scattering $I(0)$ becomes

$$I(0)/c = \frac{NM_p}{N_a d_p^2}(1 + \lambda)^2 \cdot((\mu\rho_p^D + (1 - \mu)\rho_p^H + \rho_{shell}\lambda)/(1 + \lambda) - \rho_{solvent})^2. \quad [4]$$

We thank Naveena Yanamala (University of Pittsburgh) for preparation of Fig. 4*d*. This work was supported by a Sofya Kovalevskaya Award from the Zukunftsinvestitionsprogramm der Bundesregierung Deutschland and National Science Foundation Grants ITR 0225636 and CAREER CC044917.

1. Falb M, Pfeiffer F, Palm P, Rodewald K, Hickmann V, Tittor J, Oesterhelt D (2005) *Genome Res* 15:1336–1343.
2. Seidel R, Scharf B, Gautel M, Kleine K, Oesterhelt D, Engelhard M (1995) *Proc Natl Acad Sci USA* 92:3036–3040.
3. Oesterhelt D (1998) *Curr Opin Struct Biol* 8:489–500.
4. Falke JJ, Bass RB, Butler SL, Chervitz SA, Danielson MA (1997) *Annu Rev Cell Dev Biol* 13:457–512.
5. Wadhams GH, Armitage JP (2004) *Nat Rev Mol Cell Biol* 5:1024–1037.
6. Gordeliy VI, Labahn J, Moukhametzianov R, Efremov R, Granzin J, Schlesinger R, Buldt G, Savopol T, Scheidig AJ, Klare, JP, *et al.* (2002) *Nature* 419:484–487.
7. Moukhametzianov R, Klare JP, Efremov R, Baeken C, Goppner A, Labahn J, Engelhard M, Buldt G, Gordeliy VI (2006) *Nature* 440:115–119.
8. Wegener AA, Klare JP, Engelhard M, Steinhoff HJ (2001) *EMBO J* 20:5312–5319.
9. Sudo Y, Okuda H, Yamabi M, Fukuzaki Y, Mishima M, Kamo N, Kojima C (2005) *Biochemistry* 44:6144–6152.
10. Aravind L, Ponting CP (1999) *FEMS Microbiol Lett* 176:111–116.
11. Bordignon E, Klare JP, Doebber M, Wegener AA, Martell S, Engelhard M, Steinhoff HJ (2005) *J Biol Chem* 280:38767–38775.
12. Seeley SK, Weis RM, Thompson LK (1996) *Biochemistry* 35:5199–5206.
13. Kim KK, Yokota H, Kim SH (1999) *Nature* 400:787–792.
14. Surette MG, Stock JB (1996) *J Biol Chem* 271:17966–17973.
15. Levit MN, Grebe TW, Stock JB (2002) *J Biol Chem* 277:36748–36754.
16. Liu Y, Levit M, Lurz R, Surette MG, Stock JB (1997) *EMBO J* 16:7231–7240.
17. Christian JH, Waltho JA (1962) *Biochim Biophys Acta* 65:506–508.
18. Lai MC, Gunsalus RP (1992) *J Bacteriol* 174:7474–7477.
19. Cendrin F, Chroboczek J, Zaccai G, Eisenberg H, Mevarech M (1993) *Biochemistry* 32:4308–4313.
20. Higgins JS, Benoit H (1994) *Polymers and Neutron Scattering* (Clarendon, Oxford).
21. Guinier A, Fournet G (1955) *Small Angle Scattering of X-Rays* (Wiley, New York).
22. Beaucage G (1996) *J Appl Crystallogr* 29:134–146.
23. Svergun DI, Richard S, Koch MH, Sayers Z, Kuprin S, Zaccai G (1998) *Proc Natl Acad Sci USA* 95:2267–2272.
24. Jacrot B (1976) *Rep Progr Phys* 39:911–953.
25. Hirst JD, Brooks CL, III (1994) *J Mol Biol* 243, 173–178.
26. Sreerama N, Woody RW (2004) *Methods Enzymol* 383:318–351.
27. Gokce I, Woody RW, Anderluh G, Lakey JH (2005) *J Am Chem Soc* 127:9700–9701.
28. Zagrovic B, Lipfert J, Sorin EJ, Millett IS, van Gunsteren WF, Doniach S, Pande VS (2005) *Proc Natl Acad Sci USA* 102:11698–11703.
29. Long DG, Weis RM (1992) *Biochemistry* 31:9904–9911.
30. Bonnete F, Madern D, Zaccai G (1994) *J Mol Biol* 244:436–447.
31. Le Moual H, Koshland DE, Jr (1996) *J Mol Biol* 261:568–585.
32. Grabarek Z, Gergely J (1990) *Anal Biochem* 185:131–135.
33. DeSilva NS, Ofek I, Crouch EC (2003) *Am J Respir Cell Mol Biol* 29:757–770.
34. Timmins PA, Zaccai G (1988) *Eur Biophys J* 15:257–268.
35. Svergun D, Barberato C, Koch MHJ (1995) *J Appl Crystallogr* 28:768–773.